

Real2USD: Scene Representations in Universal Scene Description Language

Christopher D. Hsu^{1,2} and Pratik Chaudhari¹

Abstract— Large Language Models (LLMs) can help robots reason about abstract task specifications. This requires augmenting classical representations of the environment used by robots with natural language-based priors. There are a number of existing approaches to doing so, but they are tailored to specific tasks, e.g., visual-language models for navigation, language-guided neural radiance fields for mapping, etc. This paper argues that the Universal Scene Description (USD) language is an effective and general representation of geometric, photometric and semantic information in the environment for LLM-based robotics tasks. Our argument is simple: a USD is an XML-based scene graph, readable by LLMs and humans alike, and rich enough to support essentially any task—Pixar developed this language to store assets, scenes and even movies. We demonstrate a “Real to USD” system using a Unitree Go2 quadruped robot carrying LiDAR and a RGB camera that (i) builds an explicit USD representation of indoor environments with diverse objects and challenging settings with lots of glass, and (ii) parses the USD using Google’s Gemini to demonstrate scene understanding, complex inferences, and planning. We also study different aspects of this system in simulated warehouse and hospital settings using Nvidia’s Isaac Sim. Code is available at <https://github.com/grasp-lyrl/Real2USD>.

I. INTRODUCTION

For tasks ranging from search and rescue, industrial automation, and guiding people through complex environments like airports or museums, a majority of robotic systems use metric representations of the environment for mapping and navigation. Humans use more abstract representations for such tasks. Structures such as place cells and grid cells in the brain [1, 2] encode space efficiently [3] and are tuned to sensory and contextual cues [4, 5]. These structures have also been argued to represent semantics for more general kinds of decision making [6]. The hallmark of human representations of space is indeed their semantic richness—often in lieu of metric details. It stands to reason that robots will benefit by combining semantic information with metric information for building effective representations of space.

This perspective is also a popular line of thought in recent literature. Bootstrapped by Large Language Models (LLMs), there are a number of techniques to augment metric representations such as voxel grids, point-clouds, signed distance functions etc. using language-based priors. These approaches work well but they are often tailored to specific tasks, e.g., visual-language models for navigation, language guided neural radiance fields for mapping, etc. See Sec. II.

We argue that the Universal Scene Description (USD) language is a general and effective representation of geometric,

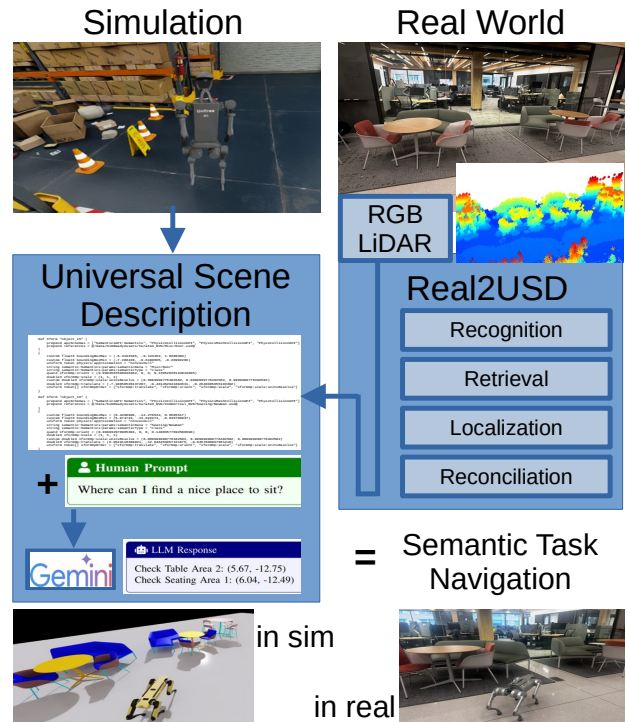


Fig. 1: In simulation, we can use the underlying USD in Isaac Sim [7] along with a task prompt with an LLM to obtain a list of waypoints for a robot as it performs complex semantical tasks such as “Find all things that might be useful in case of an emergency”. In the real world, we propose a framework called Real2USD (see Fig. 4) to build a faithful USD representation of the scene from sensor measurements (RGBD camera and pose estimates). Using this USD, a Unitree Go2 robot can perform semantic tasks in challenging indoor environments.

photometric and semantic information in the environment for LLM-based robotics tasks. A USD is an XML-based scene graph, readable by LLMs and humans alike, and rich enough to support essentially any task—Pixar developed this language to store assets, scenes and even movies [8]. This is a natural avenue compared to augmenting existing representations of the scene and retrofitting downstream tasks to work effectively with LLMs. A USD is a hierarchical scene graph.

The contributions of this work are depicted in Fig. 1 and are as follows. We demonstrate a “Real to USD” system using a Unitree Go2 quadruped robot carrying LiDAR and a RGB camera that (i) builds an explicit USD representation of indoor environments with diverse objects and challenging settings with lots of glass, and (ii) parses the USD using Google’s Gemini to demonstrate scene understanding, complex inferences, and planning. We also study different aspects of this system in simulated warehouse and hospital settings

¹Department of Electrical & Systems Engineering and General Robotics, Automation, Sensing and Perception (GRASP) Laboratory at the University of Pennsylvania. chsu8@upenn.edu, pratikac@upenn.edu

²DEVCOM Army Research Laboratory christopher.d.hsu.civ@army.mil

using Nvidia’s Issac Sim.

II. RELATED WORK

3D Metric-Semantic Scene Graph-based approaches first construct a geometric representation of the scene using simultaneous localization and mapping (SLAM) [9], structure from motion [10], or newer techniques such as neural radiance fields (NeRFs) and Gaussian splatting (3DGS) [11, 12]. This geometric map can be modified to incorporate information of object categories and semantics such as couch, book, desk, etc. [13–15]. While some approaches represent this information implicitly, e.g., a instance/category-wise segmentation of a point-cloud, some others abstract the map into a scene graph [16–18] with nodes and edges that connect the geometry to higher level concepts such as categories and relationships [19–21]. Some methods also use LLMs [22, 23] to model explicit relationships between objects in the scene. Approaches such as SLAM++ [24] also optimize the pose graph using a limited set of manually scanned objects. These “metric-semantic” representations can support planning and task execution [23, 25].

Our work follows a largely similar recipe as that of the above methods but it represents the scene graph differently. The Universal Scene Description (USD) language can represent geometric (size, shape, pose) and photometric (color, texture) properties of individual objects. It can also describe a scene using references to object-level USD and relative poses with the scene. A USD is fundamentally a hierarchical scene graph. As opposed to unstructured meshes, implicit/explicit NeRF/3DGS representations, the USD is an explicit representation with structured assets. Our mapping solution using USDs is more general than existing approaches. We search large databases of object models using deep learning-based semantic segmentation [26, 27] and foundation models such as CLIP [28]. Our argument is that the XML-based USD format is better than existing, non-standard, scene graph representations. USDs already have all the necessary functionality, e.g., support for localization, collision checking, semantic tasks, etc. And perhaps the most important benefit of this choice is that the text-based scene graph can be easily parsed by LLMs, e.g., we do not need procedures to annotate that a particular group of objects is an office (say via CLIP)—the LLM can easily infer such semantics, and much more, from the scene graph.

Real to Sim to Real was first studied as “virtualized reality” by Takeo Kanade and colleagues in 1997 to create immerse experiences of real-world events using multi-baseline stereo across 51 cameras [29]. This idea has again become important because exploiting simulation-based methods in robotics requires that we have effective methods to build realistic virtual versions of physical scenes. For example, [30, 31] use 3DGS to reconstruct the robot workspace as a mesh and import it into a physics simulator. Although a mesh is a more general scene representation than a USD that is used in this work, the former does not give accurate geometry (with limited views) and lack any articulation that a pre-built asset might have. The authors in [32] improve upon this to introduce a manual tool to segment the 3DGS representation and annotate articulations. Works like [33] take a different approach, they import articulated assets in a

3D simulation using a single RGB image as input to obtain very impressive results; others use text prompts [34–36] for synthesizing procedural scenes. SceneScript [37] uses Aria glasses for scene reconstruction via volumetric primitives, while Cubify Anything [38] does 3D object detection on more cluttered scenes. Works like [39, 40] use simulators to aid the generation of assets.

Our work has some technical similarities to this body of work, but we go beyond a single image or text prompt, and work with much larger scenes to conduct real-world experiments that last 10–15 minutes. Our mapping solution is much faster (in spite of multiple large models being queried at each instant), consistent across multiple views (in spite of occlusions and new object types), and can build maps that are compatible for physics simulators in an online fashion.

III. SEMANTIC TASKS IN SIMULATION USING A KNOWN USD REPRESENTATION OF THE SCENE

We will first demonstrate semantic navigation tasks in simulation using the ground-truth USD representation of the scene. Our goal is to show that USD, when combined with LLMs, is a sufficient representation for performing ambiguously-prescribed tasks in semantically rich environments across long time-horizons and large scenes that contain hundreds of unique assets.

These simulation experiments focus on two scenes, a warehouse and a hospital floor. We use Isaac Sim and MobilityGen [41] to work with sensor streams (RGBD and pose) and control commands of simulated Unitree H1 humanoid and Boston Dynamics Spot quadruped robots. Given the ground-truth USD of the scene, the goal is to use an LLM (Gemini via an API call) to generate a list of waypoints (position and orientation) in the world frame, and use classical planning and control to navigate the robot. The prompt is as follows.

User: You are a navigation assistant that helps plan paths to objects in a scene. The context includes a USD file that represents a snapshot of the scene at a specific point in time. Your task is to analyze this file and generate waypoints for navigation based on the query.

For each waypoint, provide:

- Position (x, y, z coordinates)
- Orientation (quaternion: qx, qy, qz, qw)
- A brief description of the waypoint.

If the query is about a specific object, identify that object in the scene and generate a waypoint to it. If the query is about planning a path to multiple objects, generate a sequence of waypoints. You MUST return your response in valid JSON format that matches the provided schema.

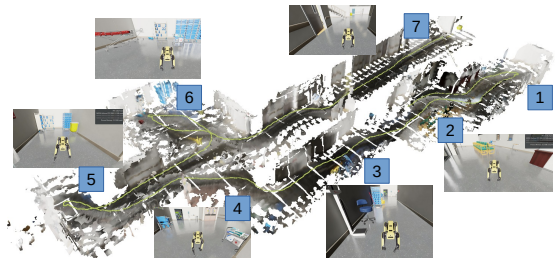


Fig. 2: Snapshots of the Spot robot at different waypoints in the hospital scene. The 3D mesh was built from simulated RGB, depth, and pose data using Khronos [42] to demonstrate coverage.

Fig. 2 shows an example where Spot navigates a hospital

UNCLASSIFIED

floor that contains 55 unique objects (1756 instances) ranging from hospital beds, soda machines, and assorted furniture (46 categories) to walls and floor descriptions (9 types). The prompt and the textual description of the waypoints is:

User: Plan a path of waypoints that navigates you around the hospital floor. Waypoints should fall within the main hospital walls but not within ANY of the objects in the USD. Be sure to choose waypoints that view some interesting objects and areas.
 Robot: Description: Planned path around the hospital floor, including interesting objects and equipment along the route.
 1. Start near the entrance, view the reception desks.
 2. Move towards the water dispenser and pharmacy area.
 3. Navigate near the chairs, side tables and scale.
 4. Head towards the area with multiple shelves and supply carts.
 5. Move to a larger area with water dispenser, side table and trashcan.
 6. Navigate towards the gurney and medical bags.
 7. Final waypoint.

We have not shown the 2D Euclidean coordinates returned by Gemini that are used for waypoint-based planning. Spot travels a distance of 128 m during this experiment with minimal backtracking and traverses a majority of the scene. Approximately 81% of the scene is observed (2371 out of 2922 m²). A majority of the unobserved scene is due to closed doors in the environment which are not traversable in our current setup.

User: Plan a path of waypoints that navigates you around the warehouse floor. Waypoints should fall within the main warehouse walls. I want you to navigate to all the useful things that would be needed in case of an emergency.
 Robot: Description: Navigating the Warehouse Floor and visiting useful things for emergency
 1. Waypoint to see the sign C ver object.
 2. Waypoint to the Emergency Board Full.
 3. Waypoint to a Fire Extinguisher near the wall.
 4. Waypoint to another Fire Extinguisher and a wet floor sign.
 5. Waypoint to another Fire Extinguisher near the shelf.
 6. Waypoint near SM_PillarA_9M objects.

With essentially the same prompt (shown above), the simulated Unitree H1 robot can search for things in a warehouse that could be useful in an emergency, see Fig. 3. The warehouse scene is approximately 1687 m² with 45 unique objects such as a forklift, boxes and crates. The robot obtains data from all 4 corners of the scene but does not enter some of the aisles. In this experiment, the robot traveled a distance of 174.1 m with substantial amounts of backtracking. Reordering waypoints given by Gemini would reduce this path length.

IV. METHODS

We next describe our pipeline (Fig. 4) to construct USD representations from sensory data collected by robots in real-world indoor environments. There are three main components: recognition and retrieval which involves using image segmentation models to identify and robustly query a database of assets (Sec. IV-A), placing these objects into the scene correctly (Sec. IV-B) and reconciliation to ensure that the reconstructed scene is physically realistic (Sec. IV-C).¹

¹ The narrative will contain footnotes that describe some problem-dependent “tricks” that were used to ensure a performant and reproducible pipeline.



Fig. 3: Inset images show safety equipment such as fire extinguishers and wet floor signs that were discovered by a Unitree H1 robot exploring the warehouse scene.

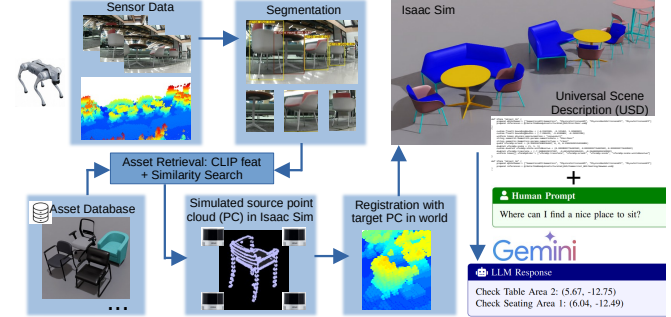


Fig. 4: We show the Real2USD pipeline where a robot collects sensor measurements and does semantic segmentation. With each image crop, it retrieves the most similar asset from our database, simulates the asset and does registration to a global point cloud. After some reconciliation, we obtain a USD in Isaac Sim that is fed to an LLM to get waypoints such that a robot can navigate to a language guided goal.

Let us first set up the problem formally. We will assume that the robot has an accurate estimate of its pose $x_t \in \text{SE}(3)$ at time t , i.e., there exists a system for localization, or odometry. Suppose the robot obtains observations $y_1^t = (y_1, \dots, y_t)$ from viewpoints x_1^t with each viewpoint x_t . An observation consists of $y_t \equiv (y_t^{\text{rgb}}, y_t^{\text{lidar}})$ which are the RGB image and point-cloud obtained from a camera and LiDAR respectively, from viewpoint x_t . The LiDAR point-cloud is registered against a global frame of reference. We want to build a representation of a static scene, denoted by ξ_t using these observations. Suppose we have a database of objects/assets $D = \{\xi^{(1)}, \dots, \xi^{(n)}\}$ (chairs, tables, doors, etc.) represented as a mesh or a textured computer-aided-design (CAD) model. We will represent the scene using these objects, i.e.,

$$\xi_t \equiv \{(\xi^{(i)}, x^{(i)})\}_{i \in \{1, \dots, n\}}. \quad (1)$$

There are $n_t \equiv |\xi_t|$ total instances of objects $\xi^{(i)}$ at poses $x^{(i)} \in \text{SE}(3)$. There can be multiple instances of the same object in $\xi^{(i)}$ but at different locations $x^{(i)}$. There are at most $|D| = n$ unique objects.

A. Asset Recognition and Retrieval

The representation of the scene ξ_t should explain the observations in y_1^t , i.e., a rendering from the scene representation should have the correct photometric and geometric properties. We are interested in semantic navigation tasks in this paper, and therefore it is not important to capture the photometric properties exactly. We now describe how to recognize and retrieve semantically-similar objects for

UNCLASSIFIED

UNCLASSIFIED

constructing the scene.

Robust object detection with open-set models. Given an RGB image, y_t^{rgb} we compute a set of putative 2D object masks and their labels using YOLOE [27, 43] shown in Fig. 5. This model can perform open-set object detection and segmentation by taking a text prompt as input. Textual prompts are useful to guide the detections onto a specific set of objects, but in indoor environments with many different objects, it is not easy to define text prompts with good recall. We therefore first run YOLOE without text prompts to use its open-set functionality. This provides us a set of putative labels which are then used to run the prompt-based YOLOE to obtain detections. This strategy results in twice as many calls to the detection model, but we found that doing so can ensure a high recall in challenging environments. It is reminiscent of constrained beam search-guided detection [44]. In contrast to using Segment Anything (SAM) [45] and CLIP to retrieve labels [28], YOLOE provides semantically consistent masks without over-segmenting objects. An approach based on SAM and CLIP could be more performant but it would require a procedure to cluster objects from parts.



Fig. 5: An example of inadequate precision and recall in open-set detection models such as YOLOE. In the left image, the couch is typically categorized as a “church bench” (dark blue). We use heuristics to map such fine-grained but semantically incorrect labels to more general labels, e.g., the “church bench” is modified to be a “chair”. Notice that the round table and desks are not segmented in these images, even with prompts such as “table” or “desk”. This inadequacy is problematic for robotics pipelines that have much more stringent requirements on their performance. We work around this by querying the model twice (see the text).

Semantic search for retrieving assets from an open-set database. Suppose we have $\{(m_t^{(i)}, l_t^{(i)}, c_t^{(i)})\}_{i=1}^m$ which are object masks (2D bounding boxes), their labels and confidence respectively, corresponding to the image y_t^{rgb} . We next retrieve objects $\xi^{(i)}$ from the database D that are semantically and geometrically consistent with these detections. We are interested in open-world settings and therefore assets in our database are not exact replicas of the objects in the real-world scene. In such cases, we should find the closest asset that matches our detections. A naive solution would use the text class label $l_t^{(i)}$ to retrieve the asset using, say, CLIP. However, within the general label of a “chair” or a “table” there are all sorts of different chairs and tables that fit those categories. Therefore, we developed our own image-based asset retrieval procedure. We use CLIP [28] to compute embeddings and a similarity search framework called FAISS [46]. In an offline process, for each USD asset in the database D , we use Issac Sim to render 4–6 views and compute their CLIP embeddings to create a FAISS vector database.² Asset retrieval is performed by embedding the image and searching for the nearest image (in terms of cosine

²We chose views that tend to match the angle for which the robot view the object, i.e., from a lower vantage point.

distance) in the vector database, and its associated object. See Fig. 6.³ We build in robustness by filtering out results that do not match the queried label.⁴ In comparison, [33] does a similar process of multiple views and CLIP for asset retrieval but further augment the process with a vision language model (VLM) which slows down retrieval. In practice we found this extra step not necessary and a bottleneck in the pipeline.

We sourced objects from Nvidia’s Omniverse SimReady Assets [47]. These assets are physically accurate 3D objects that encompass physical properties, materials, and meshes built on USD such that they can be used in simulations and behave as they would in the real world. Furthermore, we sourced CAD and REVIT models of the furniture in our scenes and converted them into “Sim Ready” USD files.

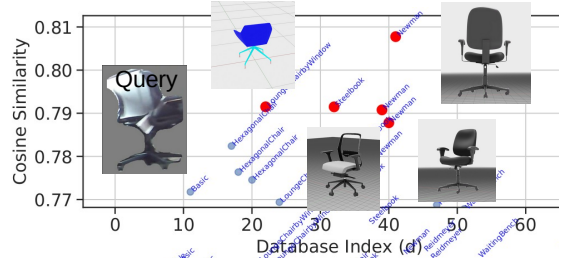


Fig. 6: Cosine similarity of a given query with objects in the database. We also visualize the top results (red points) with “Newman” (top right) being the most similar with a score of 0.808.

B. Asset Localization

Suppose we wish to place an asset $\xi^{(i)}$ into the scene in a way that is geometrically consistent with the accumulated point-cloud $\bigcup_{s=1}^t y_s^{\text{lidar}}$ in the sensor data. This involves finding the pose $x^{(i)} \in \text{SE}(3)$ for the object. This is a registration problem, and in principle, it can be solved using vertices on the mesh/CAD of the object $\xi^{(i)}$. But these vertices are typically on end-points and non-existent along flat surfaces. The point-cloud obtained from LiDAR is quite the opposite, points lie on surfaces and edges are usually absent. This puts a fundamental bound on the accuracy of registration.

A general simulation-in-the-loop approach for effective registration. We spin up a headless instance of a simulator (Isaac Sim) with the asset $\xi^{(i)}$ and obtain the point-cloud from 4 LiDARs with viewpoints that surround the object. The resulting point cloud, let us call it $\hat{y}^{(i)}$, emulates what the robot's LiDAR would have seen—but accumulated across diverse viewpoints. We cache these asset-specific point-clouds during the operation of the robot, and therefore multiple instances of the same object do not require us to instantiate the simulator again. See Fig. 7.

Registration across point-clouds and object detections. Iterative closest point (ICP) based registration between the asset's simulated point-cloud $\hat{y}^{(i)}$ and the data $\bigcup_{s=1}^t y_s^{\text{lidar}}$ can result in large aliasing because the latter represents a

³We also investigated using principal components analysis (PCA) to reduce the dimensionality of this asset retrieval, but from a qualitative evaluation, this was not necessary.

⁴Another solution would be Nvidia’s USD Search API designed for large databases. However we found it difficult to modify the views and similarity metrics because this is a closed-source framework. It also requires a Kubernetes cluster onboard the robot, and Amazon S3 a cloud-based database.

UNCLASSIFIED

UNCLASSIFIED

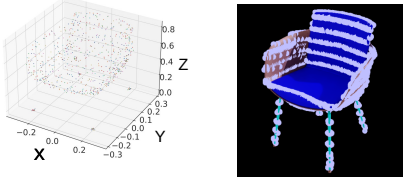


Fig. 7: Simulation-in-the-loop registration. (Left) Vertices extracted from the USD mesh of a chair. Notice how this representation lacks points along straight edges, e.g. the chair legs, which would be detrimental to point-based registration. (Right) The point-cloud that was created by simulating LiDARs and the chair in Isaac Sim.

large number of other objects. We can take advantage of the objects segmentations to improve the accuracy of registration. Assuming known camera intrinsics, we segment the entire point-cloud $\bigcup_{s=1}^t y_s^{\text{lidar}}$ to select only the LiDAR points that (when projected on the corresponding image plane) lie within object masks $\{m_s^{(i)}\}_{s \leq t}$ where the object was detected. Given this sub-sampled point-cloud and the object $\hat{y}^{(i)}$, we first use fast global registration [48] for initialization and then point-to-point ICP [49] as the second step. The former registration technique does not require initialization but we found that it is not very precise, while the latter technique can perform fine-grained registration with appropriate initialization.⁵

C. Asset Reconciliation

The previous two sections described a procedure to select assets from a database to explain the sensor observations collected from a robot. Different elements of this pipeline for detection, retrieval, registration, etc. need to be exceedingly accurate for the representation of the scene to be faithful. Even small inaccuracies in pose registration can create artifacts such as chairs intersecting with tables, doors sinking into the floor, etc. For example, state-of-the-art models for object detection have the propensity for multiple detections even with non-maximum suppression [50]. The accuracy of existing state-of-the-art perception models is not sufficient to ensure physically plausible predictions. We again take advantage of the simulation to rectify such issues.

Pruning multiple detections and incorrect registrations. Periodically, across time-steps t , we construct a k -d tree of the registered point-clouds of all n_t objects in the scene ξ_t , let us call it $\bigcup_i y_{i \in \{1, \dots, n_t\}}^{(i)}$. This helps facilitate the operations described next. The registered point-cloud can often contain multiple objects for a single real-world object, e.g., multiple chairs or tables at slightly different poses. It can also contain situations when a large object from the database, e.g., a couch, is registered to multiple smaller objects in the real-world, e.g., a chair and a table, see Fig. 8. We first prune multiple detections using non-maximum suppression (NMS) based on Euclidean position to get clusters of objects. For each cluster, we need to associate a single asset that accurately captures the point-cloud and semantics. To do so, we use a “distribution score” and a “density score” computed using the point-cloud computed via simulation-in-the-loop for an

⁵Although we do not do so in this paper due to assets generally being of correct physical scale, by including a search for scale during ICP, this approach for registration can also handle situations when objects retrieved from the database have a different size than the ones in the LiDAR point-cloud.

asset, denoted by \hat{y} here, and its intersection with the scene $\bigcup_{i \in \{1, \dots, n_t\}} \{\hat{y} \cap y^{(i)}\}$. These scores are heuristics that are designed to compute the degree to which a particular asset can explain the point-cloud corresponding to the scene. Assets within the same cluster without maximal scores are dropped, and thereby each cluster is only represented by a single asset with the maximal score.

We show an example of the scoring system in Fig. 8 which works as follows. We compute the convex hull of the point-cloud \hat{y} and discretize it into voxels of size 0.01 m. Let C be the set of with non-zero point-counts that contain the number of points corresponding to the scene that lie in each voxel. The distribution score is the coefficient of variation of these counts which measures the uniformity of the points in the hull. If μ, σ are the mean and standard deviation of the set C , then the distribution score is $1 - \frac{\sigma}{\mu}$ if $|C| > 0$. The density score is simply $|C|/\text{total voxels}$. The distribution score helps disambiguate the couch from the two chairs in the example described above. The density score helps select assets that have been registered better, i.e., it helps select for better position and orientation matches.

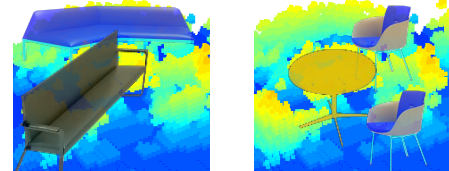


Fig. 8: Distribution and density scoring. (Left) The blue couch would have a high distribution score due to the point-cloud filling the asset uniformly in comparison to the black couch which spans two clusters. (Right) The table and the top chair would have high density scores due to being predominantly filled with points compared to the bottom chair in free space.

Using simulation to obtain a physically plausible static scene. Our approach for reconciliation of the retrieved assets helps significantly to construct a geometrically faithful representation of the scene. This is not necessarily physically faithful representation. For example, an object on top of another in the real-world might be represented using an asset that floats in mid-air. We develop a powerful trick to improve the physical plausibility of the scene representation which we show in Fig. 9. For all assets, we add rigid body and collision properties in a simulator (Isaac Sim) to instantiate the scene ξ_t . We can then forward simulate the scene to let different objects settle to their physically plausible locations, e.g., the object floating in mid-air falls down, objects that are in collision with others separate out.⁶ This is a powerful approach for ensuring that the scene representation is always physically realistic and it works well for indoor scenes without moving objects. We periodically save the USD representation of the scene for downstream scene understanding that will be described next.

V. EXPERIMENTAL EVALUATION

In this section we evaluate our mapping pipeline, Real2USD, against Clio [19]. For quantitative evaluation we

⁶We note that if the forward simulation of the scene causes an object to move to free space, the previously mentioned scoring systems will re-rank the objects in the cluster such that a potentially new object will be the best representative.

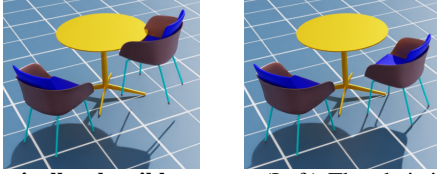


Fig. 9: Physically plausible scenes. (Left) The chair is registered partially into the table. (Right) By forward simulating the scene, the chair and table separate and the chair rests on the ground plane.

compare the bounding boxes of objects in our USD-based map to those obtained from Clio based on task descriptions in Table I. Clio is a real-time framework that uses a stereo camera for mapping and 3D scene graph creation based on task specifications. It produces 3D bounding boxes around task relevant objects using an information-theoretic framework for agglomerative clustering of object primitives with CLIP features. In order to compare, we created a ground truth dataset by manually labeling 3 scenes: small office, a hallway and a lounge.

A. Real World Data Collection

We collect data from three real-world indoor scenes: a small office, a hallway, and a lounge, by teleoperating a Unitree Go2 quadruped robot. For our method, we require a stream of RGB images, LiDAR point-cloud data collected from the Go2’s onboard Unitree L1 LiDAR, and odometry data of the robot which is estimated via the Go2’s internal system. For this method, we stream the data over WiFi via the WebRTC protocol to our main desktop. As for Clio, we mount a RealSense D435i, a stereo camera system, connected to a Nvidia Jetson NX on the back of the robot. We collect data from the RealSense on to the Jetson: RGB images, aligned depth images, and the same odometry data as previously stated. Data is stored on the Jetson and at the end of a experiment we extract the data and test Clio via playing the ROS2 bag. Both modalities of data are collected concurrently during the trajectory.

B. Real to Sim (USD)

We begin our experimental evaluation by running each method on their corresponding ROS2 bag for each scene. At the end of the experiment we extract the bounding boxes created and use them as the basis for our quantitative assessment against the ground truth labeled bounding boxes. In this experiment, we would like to observe how effective these methods are on real-world data. It should be noted that in real-world robotics experiments, image streams are not always crisp and clear as one would find from a simulator like Replica [51], Habitat [52], or Isaac Sim [7]. The camera mounted on top or in front of the robot is not stabilized during robot movement and creates motion blur as well as there is latency in processing and communication. There also are lighting changes when a robot moves towards the windows and finding depth on glass boundaries is still a common problem. Lastly, manually labeling the real world with bounding boxes is not an easy task. We collect an accumulated point-cloud of the scenes and with a 3D bounding box tool, we bound and label the point-clouds with generic labels such as chair or table. With these caveats in mind, we describe the metrics that will be reported.

a) Quantitative Results of 3D Metric-Semantic Mapping:

We would like to evaluate the effectiveness of the semantic mapping as it pertains to metric accuracy of object locations and their spatial geometry as well as identifying the correct semantic class. The nature of the semantic labels we retrieve from our method differs from that of Clio. Clio is task-driven and therefore we provide tasks such as “an image of a {class}”. Boxes that are grouped with a certain tasks will therefore directly correspond to the ground truth (gt) bounding box labels. As for our method, we label objects by the true name of the USD asset that has been retrieved. Therefore for every object type in our resulting USD we map it to a generic semantic label such that a fair comparison can be made, i.e. a Steelbook desk chair and a barstool are both “chairs”.

For each semantic class i in Table I, we calculate 3 main metrics using the predicted (pred) axis aligned bounding box, its corresponding centroid, and ground truth bounding boxes. We define Strict Accuracy (sAcc) as the ratio of instances where both the predicted centroid and the ground truth centroid is contained in the hull of the other’s box divided by the number of ground truth boxes. Relaxed Accuracy (rAcc) as the ratio of only one centroid being contained in the other. Finally, we have intersection over union: $IoU = \text{Area}_{xy}(B_{pred} \cap B_{gt}) / \text{Area}_{xy}(B_{pred} \cup B_{gt})$.

| Room | Method | chair | | | | table | | | | door | | | |
|--------------|--------|--------|--------|--------|-------|--------|--------|--------|------|--------|--------|--------|------|
| | | mIOU ↑ | sAcc ↑ | rAcc ↑ | #obj | mIOU ↑ | sAcc ↑ | rAcc ↑ | #obj | mIOU ↑ | sAcc ↑ | rAcc ↑ | #obj |
| small office | Clio | 0.079 | 0.25 | 0.25 | 2/4 | 0.0 | 0.0 | 0.0 | 0/2 | 0.0 | 0.0 | 0.0 | 1/1 |
| | Ours | 0.320 | 0.5 | 0.5 | 6/4 | 0.0 | 0.0 | 0.0 | 0/2 | 0.147 | 1.0 | 1.0 | 1/1 |
| hallway | Clio | 0.042 | 0.091 | 0.212 | 15/3 | 0.022 | 0.0 | 0.167 | 1/6 | 0.0 | 0.0 | 0.0 | 6/14 |
| | Ours | 0.187 | 0.242 | 0.394 | 24/33 | 0.051 | 0.167 | 0.167 | 3/6 | 0.029 | 0.071 | 0.071 | 4/14 |
| lounge | Clio | 0.005 | 0.034 | 0.276 | 19/29 | 0.0 | 0.0 | 0.0 | 8/7 | 0.0 | 0.0 | 0.0 | 9/2 |
| | Ours | 0.153 | 0.207 | 0.379 | 35/29 | 0.00 | 0.0 | 0.0 | 5/7 | 0.0 | 0.0 | 0.0 | 3/2 |

TABLE I: Per class metrics for 3 scenes comparing Clio against ours. For mean intersection over union (mIOU), strict accuracy (sAcc), and relaxed accuracy (rAcc), we report the mean over the class. We also report the number of each class instance compared to the number of ground truth labeled object instances per class.

First, we observe that Clio has a tendency to over cluster objects due to the ambiguity between multiple instances of a single class, i.e. a group of chairs will be clustered into a single large “chair” bounding box making it hard to make distinctions between entities. This happens because repetitive objects will have near similar CLIP embeddings which when in close proximity, the clustering algorithm will associate as one object. This deficiency is reflected in the fact that Clio has a tendency to do well on relaxed accuracy but lacks in strict accuracy or IOU. The number of Clio instances of each class is also small. In comparison, we see that our method is able to produce more focused object detections in situations where objects of similar semantic categories are close together.

We note that doors are difficult category to localize especially in this office building because they are paned with glass. What we can see from the results is that the segmentation model is able to classify a number of doors but neither method is really able to localize them well. This is due to LiDAR and RealSense depth struggling with glass. We decided to include this semantic class because we feel that for a robot, identifying these objects is essential for useful robots and we leave it for future work.

b) Qualitative Results: For each of the 3 scenes (small office, hallway, and lounge), we show in Fig. 10 the qualitative

UNCLASSIFIED

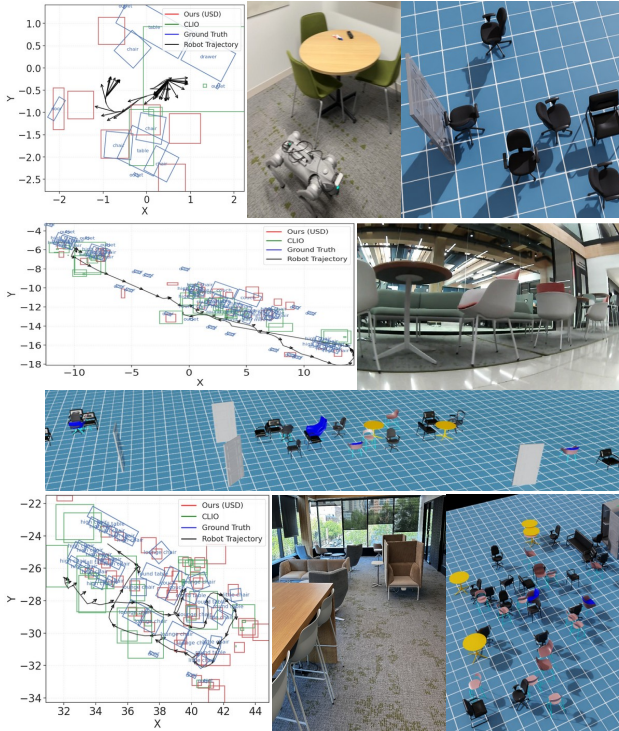


Fig. 10: We plot the 2D axis aligned bounding boxes of the objects on interest (chairs, tables, and doors) for small office (top), hallway (middle), and lounge (bottom). Blue is the ground truth, red is our method, green is Clio, and the black line with arrows show the pose of the Go2 during data collection. Figures with the blue grid are Isaac Sim renderings of the USD created by our method accompanied by an image of the real scene.

results of our method compared against Clio and the ground truth. We plot the 2D axis-aligned bounding boxes of each method and the trajectory (black lines and arrows denoting pose) the Go2 traversed during teleoperated data collection. We notice that our method does a good job of localizing objects in occupied space, whereas Clio bounds the free space in between semantically similar objects, i.e. a cluster of multiple chairs will have a large single bounding box. Our method, however, finds difficulty with partial observations. For example, if we observe only part of a couch, there are two possibilities that might occur. First, it could retrieve a couch correctly but register it incorrectly due to the masked target point-cloud. Secondly, it could retrieve a chair but a chair will only occupy a portion of the true target point-cloud. We visualize this in Fig. 8 (right) where the top chair is registered to the couch point-cloud. One can observe the issues we have with glass in each of the examples. In the small office (top), observe the chair localized next to the door on the left side, this is due to the reflection of a chair in the glass of the door. Due to our forward physics sim, the chair is pushed out into free space. In the hallway (middle), we have a few objects localized around (6, -12) which are chairs that are observed and localized as reflections in the glass or observing the chairs in the office behind the glass. Similarly in the lounge (bottom), the errant objects localized around (-30, 44) are due to reflections off of the windows (which can be seen in the real image at the back of the room).

Finally, we showcase an example of semantic navigation in our hallway scene. We query the following prompt with the

corresponding LLM response. After receiving the response, the Go2 performs waypoint based path planning and controls via Nav2 [53] to move to each of the waypoints.

User: We would like to know how many offices are connected to this hallway. The doors to the offices might not be provided in the data, where might they be? Provide some waypoints of where the robot should go for doors that might not have been seen. Note that waypoints should be given as (x,y).

Robot: 1. Extracting Relevant Coordinates

The xformOp:translate values in the USD give us the (x, y, z) coordinates of the objects. We'll use the x and y components to define our waypoints. Here's how we can extract coordinates for some key objects to guide our search:

Doors: object_301: (-0.53, -12.87), object_50: (-6.32, -10.07), object_214: (8.73, -16.94)

Seating Areas (to check nearby): object_271: (13.42, -14.53), object_160: (6.04, -12.49), object_38: (-7.55, -6.90)

Tables (to check opposite walls): object_158: (5.68, -12.75), object_39: (-7.82, -5.95)

2. Robot Search Waypoints (x, y)

Here's a set of waypoints for the robot to follow, incorporating the object locations and a systematic search pattern:

Start: (0, 0) - Assuming this is a reasonable origin point.

Check Door 1: (-0.5, -12.9) - Slightly offset from object_301.

Check Table Area: (-7.8, -6.0) - Near object_39.

Check Door 2: (-6.3, -10.1) - Slightly offset from object_50.

Check Table Area 2: (5.7, -12.8) - Near object_158.

Check Seating Area 1: (6.0, -12.5) - Near object_160.

Check Seating Area 2: (13.4, -14.5) - Near object_271.

Explanation of Strategy: We start at an origin. We visit the known door locations. We systematically traverse the hallway in a clockwise direction. We check areas near seating and tables, as these might be near entrances to other rooms. This set of waypoints provides a comprehensive search pattern, increasing the likelihood of finding both known and unknown doors.

Observe that Gemini can discern from our general task of searching for offices that it must extract locations of doors, seating areas (which are not explicitly defined but rather inferred by Gemini via clusters of chairs), and tables in the hallway scene via our USD in spite of it being rather noisy, see Fig. 10 (middle). It understands that to find offices, it should navigate along the hallway and check near clusters of furniture which could lead to finding offices.

VI. DISCUSSION

Before robots begin making fully autonomous decisions, they will have humans providing the tasks. In this work, we suggest that since the most natural way for a human to command a robot is through language, our robots must be able to understand natural language guided tasks and interpret these specifications within the context of the semantic and metric information in the environment. We argued a very natural mechanism to instantiate this paradigm is to build a representation of the scene in Universal Scene Description (USD) language. A USD-based representation is concise and rich. It can represent geometric, photometric and semantic properties of the scene—it can even simulate the scene using the underlying physics. Perhaps most importantly, it can be read by large language models (LLMs) to result in a powerful framework for language-based task specifications that can interact with the scene in a very precise fashion. To that end, this paper proposes a general pipeline to build USD representations of indoor scenes from robot sensor data. We

UNCLASSIFIED

UNCLASSIFIED

showed that we can perform complex language-guided tasks with multiple robot embodiments in simulation, as well as on a quadruped Unitree Go2 in the real world.

REFERENCES

- [1] E. I. Moser, E. Kropff, and M.-B. Moser, "Place Cells, Grid Cells, and the Brain's Spatial Representation System," *Annual Review of Neuroscience*, vol. 31, pp. 69–89, July 2008.
- [2] T. Hafting, M. Fyhn, S. Molden, M.-B. Moser, and E. I. Moser, "Microstructure of a spatial map in the entorhinal cortex," *Nature*, 2005.
- [3] X.-X. Wei, J. Prentice, and V. Balasubramanian, "A principle of economy predicts the functional architecture of grid cells," *eLife*, vol. 4, p. e08362, Sept. 2015.
- [4] Z. Wang, R. W. Di Tullio, S. Rooke, and V. Balasubramanian, "Time Makes Space: Emergence of Place Fields in Networks Encoding Temporally Continuous Sensory Experiences," in *NeurIPS 2024*, 2024.
- [5] Z. Wang, G. *Morris, D. *Derdikman, P. *Chaudhari, and V. *Balasubramanian, "REMI: Reconstructing episodic memory during intrinsic path planning," *arXiv preprint arXiv:2507.02064 (under review at NeurIPS)*, 2025.
- [6] R. Kaplan and K. J. Friston, "Entorhinal transformations in abstract frames of reference," *PLoS biology*, vol. 17, no. 5, p. e3000230, 2019.
- [7] NVIDIA, "Isaac sim." <https://github.com/isaac-sim/IsaacSim>.
- [8] Pixar-Animation-Studios, "Universal scene description (openusd)," 2016.
- [9] C. Cadena, L. Carlone, H. Carrillo, Y. Latif, D. Scaramuzza, J. Neira, I. Reid, and J. J. Leonard, "Past, present, and future of simultaneous localization and mapping: Toward the robust-perception age," *IEEE Transactions on Robotics*, vol. 32, p. 1309–1332, Dec. 2016.
- [10] O. Enqvist, F. Kahl, and C. Olsson, "Non-sequential structure from motion," in *2011 IEEE International Conference on Computer Vision Workshops (ICCV Workshops)*, pp. 264–271, 2011.
- [11] H. Oleynikova, Z. Taylor, M. Fehr, R. Siegwart, and J. Nieto, "Voxblox: Incremental 3d euclidean signed distance fields for on-board mav planning," in *IEEE/RSJ IROS*, 2017.
- [12] B. Kerbl, G. Kopanas, T. Leimkühler, and G. Drettakis, "3d gaussian splatting for real-time radiance field rendering," 2023.
- [13] S. L. Bowman, N. Atanasov, K. Daniilidis, and G. J. Pappas, "Probabilistic data association for semantic slam," in *IEEE ICRA*, 2017.
- [14] A. Rosinol, M. Abate, Y. Chang, and L. Carlone, "Kimera: an open-source library for real-time metric-semantic localization and mapping," 2020.
- [15] X. Liu, J. Lei, A. Prabhu, Y. Tao, I. Spasojevic, P. Chaudhari, N. Atanasov, and V. Kumar, "Slideslam: Sparse, lightweight, decentralized metric-semantic slam for multi-robot navigation," 2024.
- [16] I. Armeni, O. Sener, A. R. Zamir, H. Jiang, I. Brilakis, M. Fischer, and S. Savarese, "3d semantic parsing of large-scale indoor spaces," in *IEEE CVPR*, pp. 1534–1543, 2016.
- [17] U.-H. Kim, J.-M. Park, T.-j. Song, and J.-H. Kim, "3-d scene graph: A sparse and semantic representation of physical environments for intelligent agents," *IEEE Transactions on Cybernetics*, vol. 50, p. 4921–4933, Dec. 2020.
- [18] J. Wald, H. Dhamo, N. Navab, and F. Tombari, "Learning 3d semantic scene graphs from 3d indoor reconstructions," 2020.
- [19] D. Maggio, Y. Chang, N. Hughes, M. Trang, D. Griffith, C. Dougherty, E. Cristofalo, L. Schmid, and L. Carlone, "Clio: Real-time task-driven open-set 3d scene graphs," 2024.
- [20] A. Rosinol, A. Violette, M. Abate, N. Hughes, Y. Chang, J. Shi, A. Gupta, and L. Carlone, "Kimera: from slam to spatial perception with 3d dynamic scene graphs," 2021.
- [21] N. Hughes, Y. Chang, and L. Carlone, "Hydra: A real-time spatial perception system for 3d scene graph construction and optimization," 2022.
- [22] Q. Gu, A. Kuwajerwala, S. Morin, K. M. Jatavallabhula, B. Sen, A. Agarwal, and et al., "Conceptgraphs: Open-vocabulary 3d scene graphs for perception and planning," 2023.
- [23] K. Rana, J. Haviland, S. Garg, J. Abou-Chakra, I. Reid, and N. Suen-denhauf, "Sayplan: Grounding large language models using 3d scene graphs for scalable robot task planning," 2023.
- [24] R. F. Salas-Moreno, R. A. Newcombe, H. Strasdat, P. H. Kelly, and A. J. Davison, "Slam++: Simultaneous localisation and mapping at the level of objects," in *2013 IEEE Conference on Computer Vision and Pattern Recognition*, pp. 1352–1359, 2013.
- [25] D. Ong, Y. Tao, V. Murali, I. Spasojevic, V. Kumar, and P. Chaudhari, "Atlas navigator: Active task-driven language-embedded gaussian splatting," 2025.
- [26] J. Redmon, S. Divvala, R. Girshick, and A. Farhadi, "You only look once: Unified, real-time object detection," 2016.
- [27] A. Wang, L. Liu, H. Chen, Z. Lin, J. Han, and G. Ding, "Yoloe: Real-time seeing anything," 2025.
- [28] A. Radford, J. W. Kim, C. Hallacy, A. Ramesh, G. Goh, S. Agarwal, G. Sastry, A. Askell, P. Mishkin, J. Clark, G. Krueger, and I. Sutskever, "Learning transferable visual models from natural language supervision," 2021.
- [29] T. Kanade, P. Rander, and P. J. Narayanan, "Virtualized reality: Constructing virtual worlds from real scenes," *IEEE Multimedia*, vol. 4, pp. 34 – 47, January 1997.
- [30] X. Li, J. Li, Z. Zhang, R. Zhang, F. Jia, T. Wang, H. Fan, K.-K. Tseng, and R. Wang, "Robogsim: A real2sim2real robotic gaussian splatting simulator," 2024.
- [31] H. Lou, Y. Liu, Y. Pan, Y. Geng, J. Chen, W. Ma, C. Li, L. Wang, H. Feng, L. Shi, L. Luo, and Y. Shi, "Robo-gs: A physics consistent spatial-temporal model for robotic arm with hybrid representation," 2024.
- [32] M. Torne, A. Simeonov, Z. Li, A. Chan, T. Chen, A. Gupta, and P. Agrawal, "Reconciling reality through simulation: A real-to-sim-to-real approach for robust manipulation," 2024.
- [33] T. Dai, J. Wong, Y. Jiang, C. Wang, C. Gokmen, R. Zhang, J. Wu, and L. Fei-Fei, "Automated creation of digital cousins for robust policy learning," 2024.
- [34] M. Deitke, E. VanderBilt, A. Herrasti, L. Weihs, J. Salvador, K. Ehsani, W. Han, E. Kolve, A. Farhadi, A. Kembhavi, and R. Mottaghi, "Procthor: Large-scale embodied ai using procedural generation," 2022.
- [35] F.-Y. Sun, W. Liu, S. Gu, D. Lim, G. Bhat, F. Tombari, M. Li, N. Haber, and J. Wu, "Layoutlvm: Differentiable optimization of 3d layout via vision-language models," 2025.
- [36] Y. Lin, J. Humplik, S. H. Huang, L. Hasenclever, F. Romano, S. Saliceti, D. Zheng, and et al., "Proc4gem: Foundation models for physical agency through procedural generation," 2025.
- [37] A. Avetisyan, C. Xie, H. Howard-Jenkins, T.-Y. Yang, S. Aroudj, and et al., "Scenescript: Reconstructing scenes with an autoregressive structured language model," 2024.
- [38] J. Lazarow, D. Griffiths, G. Kohavi, F. Crespo, and A. Dehghan, "Cubify anything: Scaling indoor 3d object detection," 2024.
- [39] K. Yao, L. Zhang, X. Yan, Y. Zeng, Q. Zhang, L. Xu, W. Yang, J. Gu, and J. Yu, "Cast: Component-aligned 3d scene reconstruction from an rgb image," 2025.
- [40] J. Ni, Y. Chen, B. Jing, N. Jiang, B. Wang, B. Dai, P. Li, Y. Zhu, S.-C. Zhu, and S. Huang, "Phyrecon: Physically plausible neural scene reconstruction," 2024.
- [41] NVLabs, "Mobilitygen: A diffusion model for human motion synthesis." <https://github.com/NVLabs/MobilityGen>, 2024.
- [42] L. Schmid, M. Abate, Y. Chang, and L. Carlone, "Khronus: A unified approach for spatio-temporal metric-semantic slam in dynamic environments," in *RSS*, 2024.
- [43] G. Jocher, J. Qiu, and A. Chaurasia, "Ultralytics YOLO," Jan. 2023.
- [44] P. Anderson, B. Fernando, M. Johnson, and S. Gould, "Guided open vocabulary image captioning with constrained beam search," *arXiv preprint arXiv:1612.00576*, 2016.
- [45] A. Kirillov, E. Mintun, N. Ravi, H. Mao, C. Rolland, L. Gustafson, T. Xiao, S. Whitehead, A. C. Berg, W.-Y. Lo, P. Dollár, and R. Girshick, "Segment anything," 2023.
- [46] J. Johnson, M. Douze, and H. Jégou, "Billion-scale similarity search with GPUs," *IEEE Transactions on Big Data*, vol. 7, no. 3, pp. 535–547, 2019.
- [47] N. O. D. Team, *OpenUSD Exchange Samples: Collection of samples to demonstrate the OpenUSD Exchange SDK usage for data interchange between 3D Ecosystems*, 2024.
- [48] Q.-Y. Zhou, J. Park, and V. Koltun, "Fast global registration," in *Computer Vision – ECCV 2016* (B. Leibe, J. Matas, N. Sebe, and M. Welling, eds.), (Cham), pp. 766–782, Springer International Publishing, 2016.
- [49] P. Besl and N. D. McKay, "A method for registration of 3-d shapes," *IEEE Transactions on Pattern Analysis and Machine Intelligence*, 1992.
- [50] R. Jena, L. Zhorniyak, N. Doiphode, P. Chaudhari, V. Buch, J. Gee, and J. Shi, "Beyond mAP: Re-evaluating and improving performance in instance segmentation with semantic sorting and contrastive flow," in *Proc. of CVPR*, 2023.
- [51] J. Straub, T. Whelan, L. Ma, and Y. C. et al., "The replica dataset: A digital replica of indoor spaces," 2019.
- [52] A. Szot, A. Clegg, E. Undersander, and E. W. et al., "Habitat 2.0: Training home assistants to rearrange their habitat," in *NeurIPS*, 2021.
- [53] S. Macenski, F. Martin, R. White, and J. Ginés Clavero, "The marathon 2: A navigation system," in *IROS*, 2020.

UNCLASSIFIED